# Source rupture process of the 2003 Tokachi-oki earthquake determined by joint inversion of teleseismic body wave and strong ground motion data

Yuji Yagi

*International Institute of Seismology and Earthquake Engineering, Building Research Institute, 1 Tatehara, Tsukuba, Ibaraki-ken 305-0802, Japan*

(Received November 30, 2003; Revised February 23, 2004; Accepted February 29, 2004)

The spatio-temporal slip distribution of the 2003 Tokachi-oki, Japan, earthquake was estimated from teleseismic body wave and strong ground motion data. To perform stable inversion, we applied smoothing constraints to the slip distribution with respect to time and space, and determined the optimal weights of constraints using an optimized Akaike's Bayesian Information Criterion (ABIC). We found that the rupture propagates mainly along the dip direction, and the length of the rupture area is shorter than its width. The mean rise time in the shallow asperity is significantly longer than that in the deep asperity, which might be attributed to variable frictional properties or lower strength of the plate interface at shallower depths. The average rupture velocity of deep asperity extends to the shear-wave velocity. The derived source parameters are as follows: seismic moment $Mo = 1.7 \times 10^{21}$ Nm ($Mw$ 8.0); source duration = 50 sec. We also estimated the shear stress change due to the mainshock on and around the major fault zone. It appears that many aftershocks on the plate boundary took place in and adjacent to the zones of stress increase due to the rupture of the mainshock.

**Key words:** Source rupture process, stress drop, aftershocks.

## 1. Introduction

On September 26, 2003 September 25, 2003 at 19:50 (GMT), a great thrust earthquake occurred off Tokachi (Tokachi-oki), Hokkaido, Northern Japan. Two people went missing and more than 800 people were injured. The earthquake information initially provided by the U.S. Geological Survey (USGS) is as follows: origin time = 25/07/2003 19:50:06 (UTC); epicenter = 41.78°N, 144.86°W; depth = 27 km; moment magnitude ($Mw$) = 8.1. In the Tokachi-oki region, the Pacific plate subducts toward N60°W beneath the Hokkaido region from the Chishima (Kuril) Trench at a rate of about 80 mm/year (DeMets *et al*., 1990), where large and great interpolate earthquakes occurred on 1952 ($Ms$ 8.2), 1958 ($Ms$ 8.1), 1969 ($Ms$ 7.8), and 1975 ($Ms$ 7.4). The tectonic settings and the source areas of these great earthquakes are displayed in Fig. 1. Figure 2(b) shows the aftershocks during one-week after the main-shock determined by the Japan Meteorological Agency (JMA) and the focal mechanism of the mainshock determined by the present study. The mainshock mechanism is consistent with tectonic stress buildup on the interplate boundary.

In general, the teleseismic body waves contain information on the overall moment release rate and the depth range of the rupture area, while the strong ground motion data contain most of the information on the detailed slip process in the source area. Therefore, to estimate a detailed and stable source process, it is important to use both the teleseismic body waves and the strong ground motion data. Such a model is important to estimate strong ground motion near the rupture area (e.g. Dreger and Kaverina, 2000), to calculate accurate tsunami waveforms, and to understand the spatial variation of aftershocks. For this purpose, we constructed a detailed source model of this earthquake using the teleseismic data collected by the Data Management Center of the Incorporated Research Institutions for Seismology (IRIS-DMC) plus the strong ground motion records obtained by the K-NET, National Research Institute for Earth Science and Disaster Prevention (NIED) (Kinoshita, 1998). Finally, we compared the stress change due to the mainshock with aftershocks distribution.

## 2. Data and Analysis

Teleseismic body wave ($P$-waves) data recorded at IRIS-DMC stations were retrieved via the Internet. Twelve components at 12 stations were selected from the viewpoint of good azimuthal coverage. The locations of the teleseismic stations are shown in Fig. 2(a). To perform stable inversion, we used the displacement waveform. The teleseismic body waves were windowed for 120 sec, starting 10 sec before $P$-arrival time, band-passed between 0.002 and 1 Hz, and then converted into ground displacement with a sampling time of 0.25 sec.

We also selected 36 components of strong motion data obtained from 12 accelerograph stations of K-NET, NIED. The locations of these near-source stations are shown in Fig. 2(b). The acceleration data were windowed for 100 sec, starting 5 sec before the first motion, band-passed between 0.01 and 0.5 Hz, and numerically integrated to ground displacement with a sampling time of 0.25 sec. We made time corrections so that the observed $P$-wave arrivals coincide with the theoretical arrival time for near-source stations. To correct the timing for teleseismic body wave, we performed preliminary

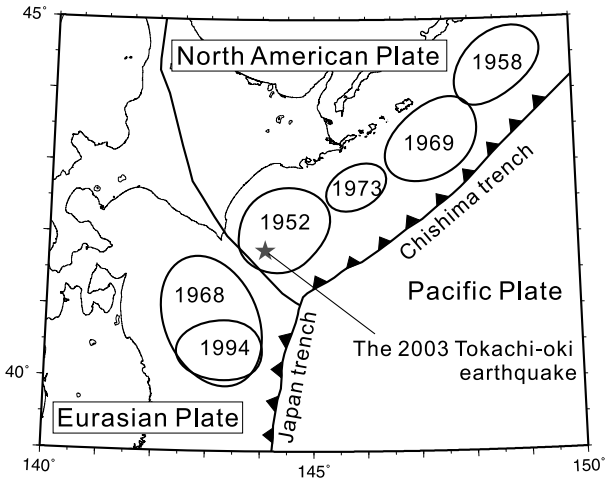


Fig. 1. Geographic map showing the epicentral location (star) of the 2003 Tokachi-oki earthquake. The contours indicate the source area of large/great earthquakes in the region (modified from Kikuchi and Kanamori, 1996).

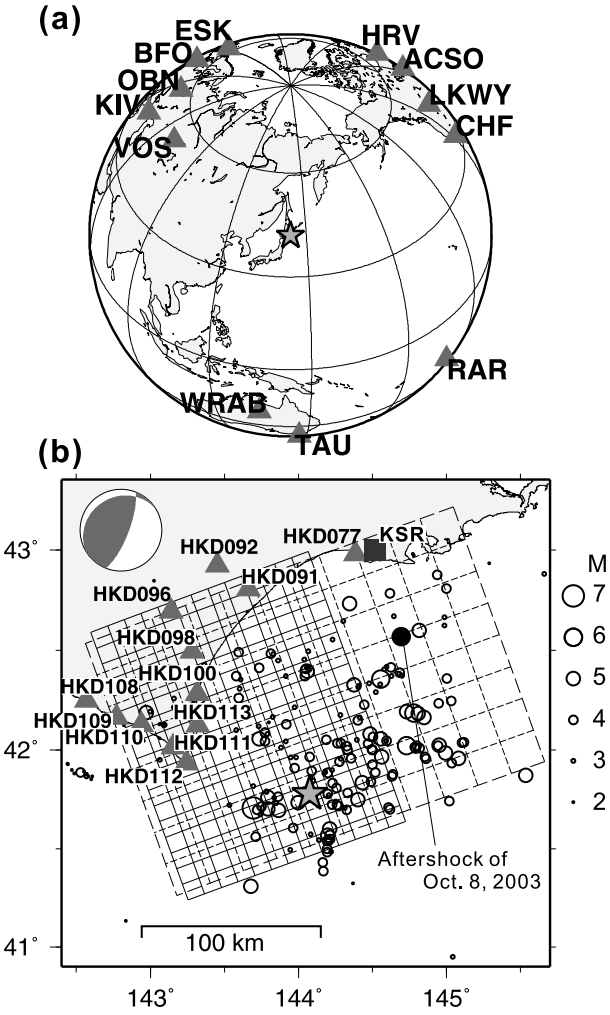


Fig. 2. (a) Teleseismic station map shown as a map view. The star represents the epicenter of the mainshock. (b) Epicenter of the mainshock (star) and aftershocks (circle) of the 2003 Tokachi-oki earthquake determined by JMA. The focal mechanism of the mainshock was determined by the present study. The K-net (NIED) stations used in the present analysis are indicated by gray triangles. The F-net (NIED) station used in the adjustment of structure model is marked by the square. The dotted and solid lines represent the assumed fault planes used in the first step and second step inversions, respectively.

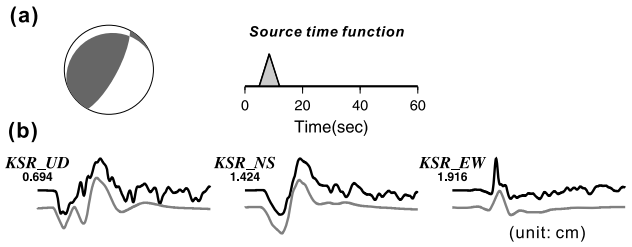


Fig. 3. (a) Assumed source time function and focal mechanism for aftershock of Oct. 8, 2003 ($Mw$ 6.5). (b) Theoretical waveforms (gray curves) from a point source and observed waveforms (black curves). The numbers below the station code indicate the maximum amplitude.

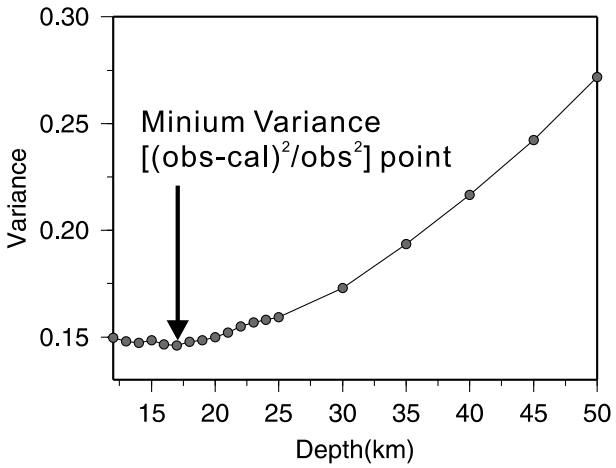


Fig. 4. Waveform variance plotted as a function of hypocentral depth. The minimum variance point (depth = 17 km) is shown.

waveform inversion using the near-source data set and calculated synthetic waveform for each teleseismic station. Later, we estimated timing corrections where the correlation coefficient between the observed and synthetic waveforms takes the maximum value.

Applying a multi-time window inversion to the data, the spatio-temporal distribution of fault slip have been estimated in previous studies (e.g. Harzell and Heaton, 1993; Yoshida, 1992). We used an inversion code originally given by Yoshida *et al.* (1992) and later developed by Yagi *et al.* (2003). In general, an increase in the number of model parameters may lead to instability of the solution, which could be affected even by a small change in the data. To obtain more stable results, we applied smoothing constraints to the slip distribution with respect to time and space. To determine the smoothness parameter objectively, we adopted the optimized Akaike's Bayesian information criterion (ABIC) (Akaike, 1980; Fukahata *et al.*, 2003, 2004).

We assumed that all points in a subfault have the same Green's function as the center of a subfault. We calculated the Green's functions for teleseismic body waves using Kikuchi and Kanamori (1991)'s method and using the discrete wave number method developed by Kohketsu (1985) for strong ground motion, respectively. The sampling time of the Green's function was set at 0.25 sec. The structure models used to compute both the teleseismic body wave and strong ground motion are given in Table 1. To ex-

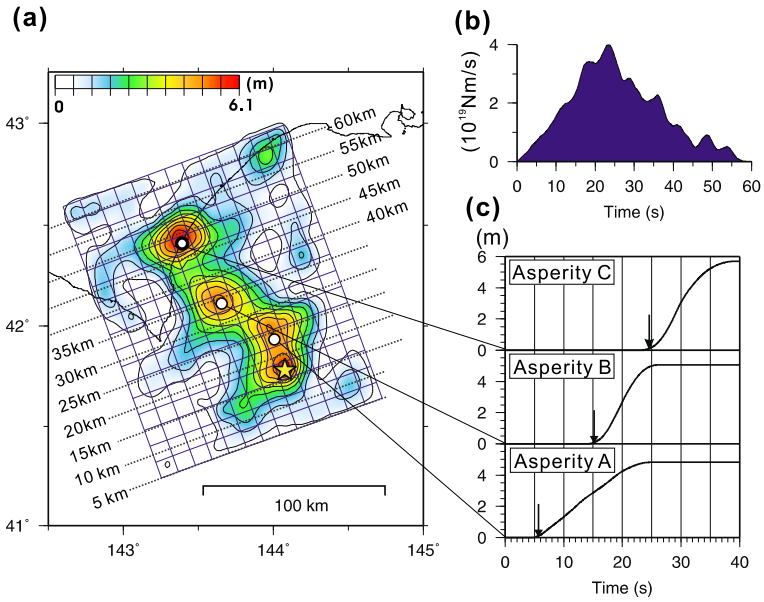


Fig. 5. Final results of joint inversion. (a) Distribution of coseismic slip on the map. The star indicates the location of the initial break. (b) Total moment-rate function. (c) Slip functions obtained in this study for each point. The arrows mark the approximate rupture propagation time estimated by the present study.

Table 1. Structure.

| Vp km/s | Vs km/s | Density $10^3$ kg/m$^3$ | Qp | Qs | Thickness (km) |
|---|---|---|---|---|---|
| For teleseismic body wave | | | | | |
| 1.5 | 0 | 1.0 | | | 1.0 |
| 3.8 | 2.19 | 2.3 | 300 | 150 | 3.0 |
| 5.5 | 3.18 | 2.6 | 500 | 250 | 4.0 |
| 5.8 | 3.34 | 2.7 | 500 | 250 | 10.0 |
| 6.5 | 3.74 | 2.9 | 600 | 300 | 10.0 |
| 7.8 | 4.5 | 3.2 | 1200 | 600 | — |
| For strong ground motion | | | | | |
| 3.8 | 2.19 | 2.3 | 300 | 150 | 4.0 |
| 5.5 | 3.18 | 2.6 | 500 | 250 | 4.0 |
| 5.8 | 3.34 | 2.7 | 500 | 250 | 10.0 |
| 6.5 | 3.74 | 2.9 | 600 | 300 | 10.0 |
| 7.8 | 4.5 | 3.2 | 1200 | 600 | — |

plain the broadband aftershock waveforms from the Tokachi-oki sequence, we modified the structure model described by Iwasaki *et al*. (1989). To adjust the structure model, we used F-net, NIED station (Fig. 2(b)). Figure 3 shows the theoretical displacement waveforms from a point source and the observed waveforms for aftershock of Oct. 8, 2003 (Mw 6.5). Location of this aftershock is displayed in Fig. 2(b). The general feature of the observed waveforms can be explained by using our structure model. We added a layer of 1-km thick for teleseismic body wave to model complicated water reverberations. Considering the quality of the observed records, we put their relative weight in such a way that the standard deviations of the strong ground motion and the far-field $P$-wave are about 10% and 10% of their own maximum amplitude, respectively.

We assumed that faulting occurred on a single fault plane. We adopted the focal mechanism of (strike, dip, rake) = (250°, 20°, 130°), and the epicenter determined by JMA (Latitude = 41.78°N; Longitude = 144.08°E). This focal mechanism was modified slightly from the USGS Fast Moment Tensor Solution to be consistent with the amplitude of $P$-waves and with the geometry of the fault plane that has been determined by the focal mechanism and seismicity (Ito *et al*., 2004). We solved the least squares problem with a positivity constraint on the model parameters using the non-negative least squares (NNLS) algorithm of Lawson and Hanson (1974).

In order to obtain gross features as well as some details of the rupture process, we divided the procedure into two steps. In the first step, we took a broad fault area of 220 km (ENE) × 160 km (NWN) to obtain a rough estimate of the effective rupture area and the depth of the hypocenter, which we divided into 11 × 8 subfaults, each with an area of 20 km × 20 km (Fig. 2). To save the computation time, we assumed a rupture front velocity ($V_i$), which gives the start time of the basis function at each sub-fault. For $V_i$, we tested a range of values between 2.5 and 4.5 km/sec, and finally found that a velocity of 4.5 km/sec shows a minimum variance. The slip-rate function on each subfault is expanded into a series of 12 triangle functions with a rise time of 2 sec. The duration of this slip-rate function may consist of the dislocation rise time and the rupture propagation time across a subfault. Since the hypocentral depth is not adequately constrained by the local seismological network, we varied the hypocentral depth from 12 to 50 km in the inversion procedure with the fault mechanism and epicenter fixed, and found its minimum variance at 17 km (Fig. 4). This depth is significantly shallower than the depth of hypocenter determined by JMA: 42 km. The effective rupture area was roughly estimated to be 100 km (ENE) × 160 km (NWN). In the second step, the fault plane was taken to have an area of 130 km (ENE) × 170 km (NWN) so that it covered the effective rupture area, which we divided into 13 × 17 subfaults, each

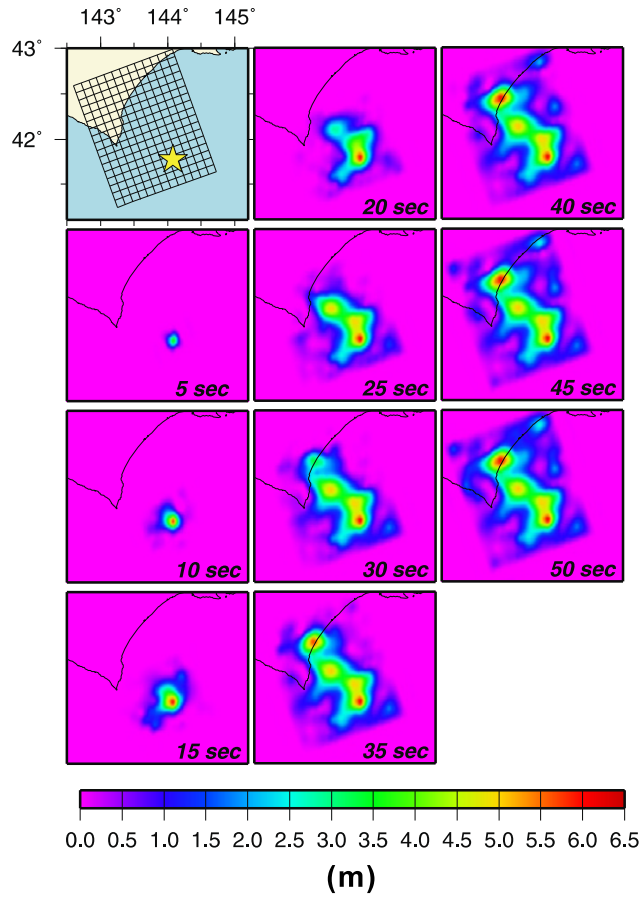


Fig. 6. Snapshots of surface projection of the dislocation at every 5 sec. The star indicates the epicenter.

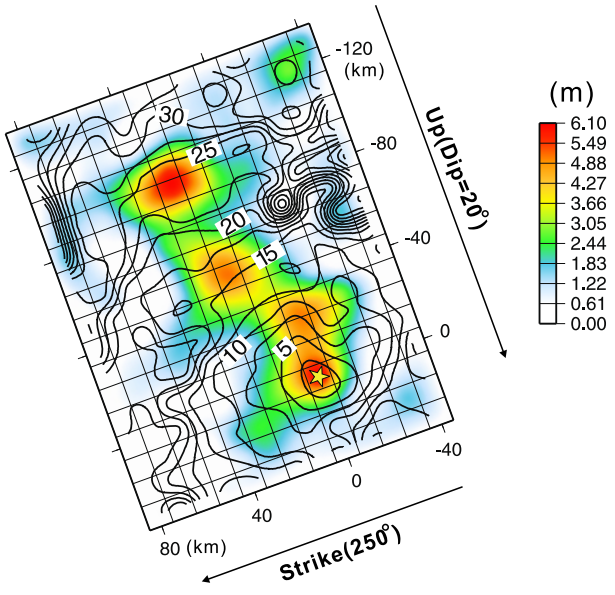


Fig. 7. The approximate rupture front motion (counter) estimated by the present study and coseismic slip on the fault plane. The counter interval is 2.5 sec.

having an area of 10 km × 10 km. The slip-rate function on each subfault is expanded into a series of 12 triangle functions with a rise time of 2 sec. The rupture front velocity is also set at 4.5 km/sec in this case.

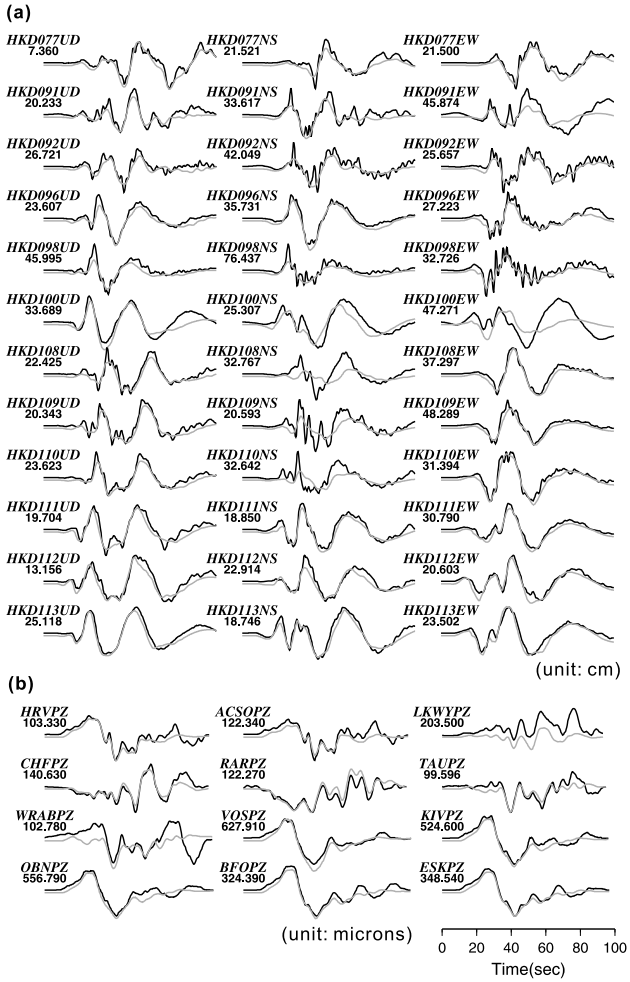


Fig. 8. Comparison of the observed waveforms (upper trace) with the calculated waveforms (lower trace). (a) Strong motion data. (b) Teleseismic body wave. The numbers below the station code indicate the maximum amplitude.

## 3. Source Model

The inversion results are shown in Figs. 5 and 6. Figure 5(a) shows the final dislocation plotted on the map. Figure 6 demonstrates a snapshot of the dislocation at every 5 sec. Figure 6 demonstrates that the rupture propagated to the northwest breaking a shallow asperity (asperity A) centered at about 15 km northwest from the epicenter during the first 15 sec. Later, the rupture propagated to the northwest and broke a middle asperity (asperity B) centered at about 60 km north-west from the epicenter during 15 to 30 sec after the initial break. Finally, the rupture propagated further to the northwest and broke a deep asperity (asperity C) centered at about 120 km north-west from the epicenter during 30 to 40 sec. The rupture propagated mainly along the dip direction, and the length along strike direction of the rupture area is shorter than its width. The maximum slip amounts to 6.1 m near the epicenter. The average estimation error corresponding to total slip is about 1.5 m. Total seismic moment is $Mo = 1.7 \times 10^{21}$ Nm ($Mw = 8.1$), which is in agreement with that of the USGS Fast Moment Tensor Solution: $1.6 \times 10^{21}$ Nm. The total source duration is about 50 sec.

The mean source time for a unit fault area (10 km × 10 km) to be ruptured is about 18 sec in the asperity A, while

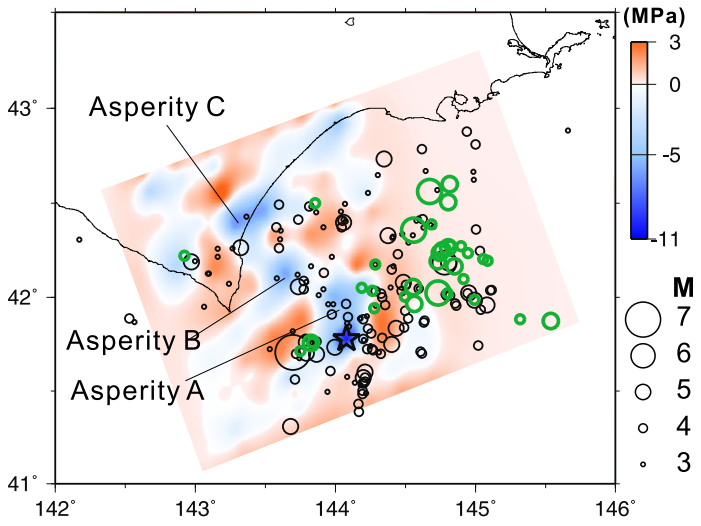


Fig. 9. Distribution of shear stress change due to the mainshock, aftershocks for the first one week after the mainshock (black circle), and the aftershocks whose nodal plane is similar to mainshock detected by Ito *et al*. (2004) (green circle). Blue and red areas indicate the zones of stress decrease and increase, respectively. The star indicates the mainshock epicenter.

the source time of the asperity B and C are about 9 and 12 sec, respectively (Fig. 5(c)). The source time may consist of the dislocation rise time and the rupture propagation time. In the present case, the rupture propagation time for a unit of fault area of 10 km in length is about 2.5sec. Therefore the mean raise time in the shallow asperity A is about 15.5 sec, which is significantly longer than that of 5.5 sec in the asperity B. The significantly longer rise time on asperity A at shallower depths is consistent with the result of the 2003 Colima earthquake (Yagi *et al*., 2003) and appears consistent with the general trend of source durations for shallow subduction earthquakes, which might be attributed to variable frictional properties or lower strength of the plate interface at shallower depths (Bilek and Lay, 2002).

To estimate the rupture velocity, we assumed that the rupture reached each sub-fault when the accumulated slip exceeds 2% of the maximum slip at each sub-fault. Figure 7 shows the rupture time thus approximated in this way. The average rupture velocity in the asperity A is about 3.0 km/sec, while that in the asperity B and C is 4.5 km/sec. The rupture velocity in the asperity B and C extends to the shear-wave velocity of the asperity B and C. The rupture velocity seems to be in proportion to the shear-wave velocity.

Figure 8 displays a comparison between the observed records (black) and the synthetics (gray). The waveform fit is good except for the horizontal components of HKD100. The horizontal component of station HKD100 seems to be contaminated by long period noise.

## 4. Coseismic Shear Stress Change and Aftershock Distribution

We also estimated the coseismic change of shear stress on and around the dipping fault plane due to the rupture process of the mainshock, to compare it with the aftershock distribution. We calculated the shear stress component parallel to the slip direction on the mainshock fault plane using the formulations for static dislocation in a homogeneous half-space (Okada, 1992). Figure 9 shows the shear stress change due to the mainshock. It is found that the maximum stress drop is 10 MPa near the epicenter. On the other hand, we noticed a zone of stress increase up to 2.3 MPa around this large stress drop zone.

The locations of aftershocks for the one-week after the mainshock are shown in Fig. 9. It is remarkable that the aftershock area expanded to the northeast from the area of coseismic slip of the mainshock. However, studies on the details of moment release distribution show that aftershocks tend to expand into the area surrounding the coseismic slip region (e.g. Mendoza and Hartzell, 1988; Takeo and Mikami, 1990; Yagi *et al*., 1999). Our results also show a similar tendency.

Ito *et al*. (2004) determined the focal mechanisms of large aftershocks using broadband seismographs and found that the aftershocks can be divided into three groups: (1) the thrust fault type whose nodal plane is similar to that of the mainshock; (2) different thrust type, and (3) the normal fault type. They also found that the depth distribution of type (1) is coincident with the plate boundary, while the depth distributions of types (2) and (3) scatter above and beneath the plate boundary. Green circles in Fig. 9 shows the aftershocks of type (1). It should be noted that the aftershock of type (1) did not occur in the large stress-drop zone, while its activity of is high at the northeast side of the large stress-drop zones, where the shear stress increases. These patterns suggest that many aftershocks on the plate boundary were triggered by stress increase due to nonuniform rupture process of the mainshock.

## 5. Summary

We constructed a detailed and stable source model of the 2003 Tokachi-oki, Japan, earthquake using the teleseismic data collected by the IRIS-DMC and the strong ground motion records obtained by the K-NET (NIED), and also estimated the shear stress change on and around the dipping fault plane due to the rupture process of the mainshock. We found that the depth of the hypocenter is about 17 km, which

is significantly shallower than the depth determined by JMA. The rupture propagates mainly along the dip direction, and the length of the rupture area is shorter than its width. The mean rise time in the shallow asperity is significantly longer than that in the deep asperity, which might be attributed to variable frictional properties or lower strength of the plate interface at shallower depths. The average rupture velocity of deep asperity extends to the shear-wave velocity. Many aftershocks on the plate boundary took place in and adjacent to the zones of stress increase due to the mainshock fault rupture.

**Acknowledgments.** The near-source data and teleseimsic body wave data used in the present study are from the National Research Institute for Earth Science Disaster Prevention and Data Management Center of the Incorporated Research Institutions, respectively. The mainshock and aftershock data have been provided by the Japan Meteorological Agency. I am grateful to Dr. S. Miyazaki, Mr. Y. Ito, Dr. Y. Asano, and Dr. S. Sekine for many valuable discussions. We also thank Prof. T. Mikumo and Dr. D. Dreger for their critical reviews.

## References

Akaike, H., Likelihood and Bayes procedure, in *Bayesian Statistics,* edited by J. M. Bernardo, M. H. DeGroot, D. V. Lindley, and A. F. M. Smith, pp. 143–166, University Press, Valencia, Spain, 1980.

Bilek, S. L. and T. Lay, Tsunami earthquakes possibly wide spread manifestations of frictional conditional stability, *Geophys. Res. Lett.*, **29**, GL015215, 2002.

DeMets, C., R. Gordon, D. Argus, and S. Stein, Current plate motion, *Geophys. J. Int.*, **101**, 425–478, 1990.

Dreger, D. and A. Kaverina, Seismic remote sensing for the earthquake source process and near-source strong shaking: A case study of the October 16, 1999 Hector Mine earthquake, *Geophys. Res. Lett.*, **27**, 1941–1944, 2000.

Fukahata, Y., Y. Yagi, and M. Matsu'ura, Waveform inversion for seismic source processes using ABIC with two sorts of prior constraints: Comparison between proper and improper formulations, *Geophys. Res. Lett.*, **30**, 10.1029/2002GL016293, 2003.

Fukahata, Y., A. Nishitani, and M. Matsu'ura. Geodetic data inversion using ABIC to estimate slip history during one earthquake cycle with viscoelastic slip-response functions, *Geophys. J. Int.*, **156**, 140–153, 2004.

Hartzell, S. H. and T. H. Heaton, Inversion of strong ground motion and teleseismic waveform data for the fault rupture history of the 1979 Imperial Valley, California earthquake, *Bull. Seism. Soc. Am.*, **73**, 1553–1583, 1993.

Ito, Y., H. Matsubayashi, H. Kimura, T. Matsumoto, Y. Asano, and S. Sekiguchi, Spatial distribution for moment tensor solutions of the 2003 Tokachi-oki earthquake ($M_{JMA} = 7.9$) and aftershocks, Earth Planets Space, **56**, this issue, 301–306, 2004.

Iwasaki, T., H. Shiobara, A. Nishizawa, T. Kanazawa, K. Suyehiro, N. Hirata, T. Urabe, and H. Shimamura, A detailed subduction structure in the Kuril trench deduced from ocean bottom seismographic refraction studies, *Tectonophysics,* **165**, 315–336, 1989.

Kikuchi, M. and H. Kanamori, Inversion of complex body wave-III, *Bull. Seism. Soc. Am.*, **81**, 2335–2350, 1991.

Kikuchi, M. and H. Kanamori, Rupture process of the Kobe, Japan, earthquake of Jan. 17, 1995, determined from teleseismic body wave, *J. Phys. Earth,* **44**, 429–436, 1996.

Kinoshita, S., Kyoshin Net (K-NET), *Seismological Research Letters,* **69**, 1998.

Kohketsu, K., The extended reflectivity method for synthetic near-field seismograms, *J. Phys. Earth,* **33**, 121–131, 1985.

Lawson, C. L. and R. J. Hanson, *Solving Least Squares Problems,* Prentice-Hall, Inc., Englewood Cliffs. New Jersey, 1974.

Mendoza, C. and S. H. Hartzell, Aftershock patterns and main shock faulting, *Bull. Seism. Soc. Am.*, **78**, 1438–1449, 1988.

Okada, A., Internal deformation due to shear and tensile faults in a half-space, *Bull. Seism. Soc. Am.*, **82**, 1018–1040, 1992.

Takeo, M. and N. Mikami, Fault heterogeneity of inland earthquake in Japan, *Bull. Earthquake Res. Inst. Univ. Tokyo*, **65**, 541–569, 1990.

Utsu, T., Space-time pattern of large earthquakes occurring off the Pacific coast of the Japanese Islands, *J. Phys. Earth,* **22**, 325–342, 1974.

Yagi, Y, M. Kikuchi, S. Yoshida, and T. Sagiya, Comparison of the coseismic rupture with the aftershock distribution in the Hyuga-nada earthquakes of 1996, *Geophys. Res. Lett.*, **26**, 3161–3164, 1999.

Yagi, Y. T. Mikumo, J. Pacheco, and G. Reyes, Source rupture process of the Tecoman, Colima, Mexico earthquake of January 22, 2003, determined by joint inversion of teleseismic body wave and near-field data, submited to Bull. Seism. Soc. Am., 2003.

Yoshida, S., Waveform inversion for rupture process using a non-flat seafloor model: application to 1986 Andreanof Islands and 1985 Chile earthquake, *Tectonophysics,* **211**, 45–59, 1992.

Y. Yagi (e-mail: yagi@kenken.go.jp)